ACADEMIC PRESS

Available online at www.sciencedirect.com
SCIENCE DIRECT®

Journal of Catalysis 214 (2003) 220–233

JOURNAL OF CATALYSIS

www.elsevier.com/locate/jcat

Behavior of bimetallic Pd–Cr/Al_2O_3 and Pd–Cr/(Ce,Zr)O_x/Al_2O_3 catalysts for CO and NO elimination

M. Fernández-García,[a,*] A. Martínez-Arias,[a] A. Iglesias-Juez,[a] A.B. Hungría,[a] J.A. Anderson,[b] J.C. Conesa,[a] and J. Soria [a]

[a] *Instituto de Catálisis y Petroleoquímica, CSIC, Campus Cantoblanco, 28049 Madrid, Spain*
[b] *Division of Physical and Inorganic Chemistry, University of Dundee, DD14HN, Dundee, Scotland, UK*

Received 29 July 2002; revised 16 October 2002; accepted 24 October 2002

Abstract

A series of Pd–Cr bimetallic catalysts supported on a (Ce,Zr)O_x/Al_2O_3 mixed support or Al_2O_3 alone have been characterized using a combination of X-ray diffraction, electron paramagnetic resonance, and Raman spectroscopy and employing in situ diffuse reflectance infra-red Fourier transform and X-ray near-edge structure spectroscopy to analyze the redox and chemical processes taking place during the course of the CO + NO + O_2 reaction. The catalytic behavior of these bimetallic systems was strongly affected by the nature of the support. In the case of the alumina support, evidence for interactions between Pd and Cr was observed in the calcined state. Under reaction conditions, formation of a mixed oxide phase containing Pd(I) and Cr(III) appears to be responsible for the improvement in CO oxidation and for the detrimental effect in the NO reduction process with respect to a monometallic, Pd reference system. In the case of the (Ce,Zr)O_x/Al_2O_3 mixed support, the addition of Cr was less influential in terms of catalytic activity. Results for the latter are rationalized mainly on the basis of the absence of interaction between the metal components in the calcined state and the presence of surface entities containing Cr alone when metallic-like Pd particles are formed during the course of reaction.

Keywords: Pd–Cr bimetallic catalysts; Pd–Cr mixed oxides; Pd–Cr alloys; CeO_2–ZrO_2; Al_2O_3; CO oxidation; NO reduction; XRD; TEM-XEDS; EPR; in situ DRIFTS; in situ XANES

1. Introduction

Three-way catalysts (TWC) have been widely used to diminish pollutant emissions from gasoline engine powered vehicles [1]. Classical components of these systems usually include Rh, Pt, and/or Pd as active metals, ceria as promoter, and high-surface alumina as support [1,2]. More recently, the classical promotion by ceria has been extended to include other oxide components in order to increase or maintain the durability of the TWC while decreasing the toxic emissions produced during the cold-start (or light-off) period, which may represent a considerable portion of the total emissions produced during any driving cycle [1,3]. Among the latter, Ce–Zr mixed oxide systems have been considered as substitutes for ceria on the basis of their greater oxygen storage capacity (OSC) after thermal sintering, which could potentially decrease the cold-start emissions, mainly by allowing the catalyst to be located in positions closer to the engine manifold with minimum system deactivation being produced [4]. Optimum promoter properties are achieved at Ce/Zr atomic ratios close to one and when pseudocubic (tetragonal symmetry for oxygen sublattice) or cubic structures of the mixed oxide are formed, which are presumably stabilized as nanosized particles [4–7]. When supported on alumina, these chemical/structural characteristics have been optimized by employing synthesis methods based on reverse microemulsions [7], rather than more classical methods based on coimpregnation [4,8,9]. The advantages induced by the use of adequate preparation methods are particularly evident when the supports are subjected to aging treatments, which degrade the tetragonal structure of mixed oxides with Ce:Zr atomic ratio close to 1 in a disproportion reaction which produces two (Ce-rich and Zr-rich) phases [7–10].

* Corresponding author.
E-mail address: m.fernandez@icp.csic.es (M. Fernández-García).

0021-9517/03/$ – see front matter
doi:10.1016/S0021-9517(02)00145-8

The use of Pd as the single active metal component in TWCs has recently received considerable attention as a result of the high cost and scarcity of Rh, the availability of cleaner fuels, and its remarkable activity for oxidation reactions [1,11]. However, some limitations are apparent for Pd-only systems with respect to their performance in NO reduction reactions [11–13]. It would be desirable to promote Pd with lower cost base metals instead of using Rh as an additional active metal, despite the latter's well-known activity for NO elimination [14]. As detailed in the review by Coq and Figueras [15], promising results have been obtained by using Mo [16,17], Mn [18], Cr [19], or Cu [20–22], which have been attributed to the formation of the corresponding alloys (with consequent perturbation of the Pd electronic properties) or, in the case of Mo or Mn, to a mixture of effects involving alloy formation (in the case of Mn) and/or the existence of Pd–$Mo^{\delta+}$, Pd–$Mn^{\delta+}$ interactions where the redox capabilities of the non-noble metal facilitate both CO activation and NO dissociation. In the case of copper, the promoting effect on both CO oxidation and NO reduction activities induced by alloying may be explained, according to theoretical studies [23], by the strong modification produced in the Pd valence electronic density by charge injection into the *sp* subband.

The case of Cr is particularly interesting as the interaction between the two active components, Pd and Cr, is present in both the oxidized and reduced states. As in the case of Cu [24], the existence of Pd–Cr mixed oxides [25] and alloys [26] is well known. However, a drastic difference can be observed between these two binary systems when the existence and stability of zerovalent solid solution phases, which are the common phases detected in TWC systems during treatment with reductive or stoichiometric mixtures are compared [19,20,22,24]. While complete mixing is obtained in the Pd–Cu case, Pd–Cr displays limited solubility in a broad region around equimolar concentration at working temperatures (below 873 K). It is clear that the extent of interaction between Pd–Cr in TWCs is largely unknown and requires attention. In this work, the objective was to address this aspect using ceria–zirconia promoted Pd–Cr catalysts, focusing on determining which are the main physical/chemical parameters affecting catalytic performance in reactions of interest for the TWC. A series of Pd–Cr bimetallic catalysts supported on Al_2O_3 and on $(Ce,Zr)O_x/Al_2O_3$ mixed supports have been studied using a multitechnique approach involving XRD, TEM-XEDS, Raman, and EPR for catalyst characterization and catalytic activity in combination with in situ DRIFTS and XANES techniques to evaluate the catalytic performance, along with the physicochemical processes which take place during the course of the stoichiometric $CO + O_2 + NO$ reaction.

2. Experimental

2.1. Catalyst preparation

A ceria–zirconia/alumina support (CZA) of 10 wt% of mixed oxide—expressed as $Ce_{0.5}Zr_{0.5}O_2$—was prepared by modification of the microemulsion method used previously for preparing the unsupported oxide [6]. Full details of the procedure can be found elsewhere [7]. After drying overnight at 373 K, this support was calcined under air at 773 K for 2 h ($S_{BET} = 186\ m^2\,g^{-1}$). According to ICP-AES chemical analysis, it has a Zr/Ce atomic ratio of 1.0 ± 0.1. This CZA support was coimpregnated (incipient wetness method) with aqueous solutions of palladium (II) and chromium (III) nitrates (from Alfa Aesar and Merck, respectively; purities > 99.99%) in an amount to give 1.0 wt% of the precious metal and varying quantities (0.25, 0.5, and 1 wt%) of the base metal. These amounts correspond to Pd:Cr atomic ratios of 0.5, 1, and 2 respectively. Monometallic references containing 1 wt% of Pd or Cr were also prepared. Three additional systems of 1 wt% of Pd, 1 wt% of Cr, and the corresponding bimetallic with 1 wt% of each metal were also prepared on the parent alumina (A; from Condea $S_{BET} = 180\ m^2\,g^{-1}$). The catalysts were calcined following the same drying/calcination procedure described above for the supports and are referred to as PdA, PdCZA, CrA, CrCZA, PdxxCrA, and PdxxCrCZA, where xx denotes the weight percentage of Cr.

2.2. Catalytic tests

Catalytic tests using stoichiometric mixtures of 1% CO + 0.45% O_2 + 0.1% NO (N_2 balance) at $30{,}000h^{-1}$ were performed in a Pyrex glass flow reactor system. Details of the experimental conditions employed for these tests can be found elsewhere [27]. Gases were regulated with mass flow controllers and analyzed using an on-line Perkin–Elmer 1725X FTIR spectrometer coupled with a multiple reflection transmission cell (Infrared Analysis Inc.; path length 2.4 m). Oxygen concentrations were determined using a paramagnetic analyzer (Servomex 540A). Experimental error in the CO and/or NO conversion values obtained in these conditions is estimated as ±7%. Prior to catalytic testing, in situ calcination was performed in diluted oxygen (2.5% O_2 in N_2) at 773 K, followed by cooling under the same atmosphere and subsequent N_2 purging at room temperature (RT). A typical test consisted of increasing the temperature from 298 to 823 K at 5 K min^{-1}.

2.3. Characterization techniques

Powder X-ray diffraction (XRD) patterns were recorded on a Siemens D-500 diffractometer using nickel-filtered Cu-K_α radiation operating at 40 kV and 25 mA and with a 0.025° step size. Transmission electron microscopic (TEM) analysis of materials was done with a JEOL 200

FX (0.31-nm point resolution) equipped with a LINK (AN10000) probe for energy dispersive X-ray spectroscopy (XEDS).

Raman spectra were acquired using a Renishaw Dispersive system 1000, equipped with a single monochromator, a holographic Notch filter, and a cooled TCD. Samples were excited using the 415 nm Ar line in an in situ cell (Linkam TS-1500), which allowed treatment under controlled atmospheres. Samples were analyzed as stored and after drying at 773 K using synthetic air; spectra consisted of 100 accumulations during 15 min acquisition time, using a typical running power of 25 mW.

EPR spectra were recorded at 77 K and room temperature (RT) with a Bruker ER 200 D spectrometer operating in the X-band and calibrated with a DPPH standard ($g = 2.0036$). Portions of ca. 40 mg of sample were placed inside a quartz probe with greaseless taps, calcined at 773 K for 1 h under 200 Torr of oxygen, evacuated at RT (1×10^{-4} Torr), and measured at liquid nitrogen temperature. Quantitative estimation of the amount of paramagnetic species was performed by double integration of the spectra and comparison with a copper sulfate pentahydrate standard.

DRIFTS analysis of adsorbed species present on the catalyst surface under reaction conditions was carried out using a Perkin–Elmer 1750 FTIR fitted with an MCT detector. Analysis of the NO conversion at the outlet of the IR chamber was performed by chemiluminescence (Thermo Environmental Instruments 42C). Additional post-catalyst gas analysis was performed using a Baltzers Prisma Quadropole mass spectrometer. The DRIFTS cell (Harrick) was fitted with CaF_2 windows and a heating cartridge that allowed samples to be heated to 773 K. Samples of ca. 80 mg were calcined in situ at 773 K (with synthetic air, 20% O_2 in N_2) and then cooled to 298 K in synthetic air before the introduction of the reaction mixture and subsequent heating at 5 K min^{-1} up to 673 K, recording one spectrum (4 cm^{-1} resolution, average of 20 scans) generally every 10–15 K. The gas mixture (using the same concentrations as those employed for laboratory reactor tests) was prepared using a computer-controlled gas blender with 75 cm^3 min^{-1} passing through the catalyst bed.

XANES experiments at the Cr and Pd K-edges were performed on line 7.1 at SRS, Daresbury (Cr K-edge), and on line BM29 of the ESRF synchrotron at Grenoble (Pd K-edge). Si(111) (for Cr) and Si(311) (for Pd) double-crystal monochromators were used in conjunction with a Pt-coated focalized mirror (7.1) or rejection mirror (BM29) to minimize the harmonic content of the beam. Additionally, a detuning of 30% was used for experiments conducted on Station 7.1. Transmission experiments were carried out using N_2/O_2 (Cr) or Kr/Ar-filled (Pd) ionization chambers. The energy scale was simultaneously calibrated by measuring the corresponding metal foil inserted before a third ionization chamber. Samples as self-supported discs (absorbance 0.5–2.0) were placed in a controlled-atmosphere cell for treatment. XANES spectra were taken every 15 K during a 5 K min^{-1} temperature ramp up to 673 K, in the presence of the $CO + NO + O_2$ flowing mixture (similar to that employed for catalytic activity tests).

Results obtained in XANES experiments were subjected to normalization using standard procedures and analyzed using principal component analysis (PCA) [28–30], which assumes that the absorbance in a set of spectra can be mathematically modeled as a linear sum of individual components, called factors, which correspond to each of the palladium or chromium species present in a sample plus noise [31]. To determine the number of individual components, an F-test based on the variance associated with factor k and the summed variance associated with the pool of noise factors is performed. A factor is accepted as a "pure" chemical species (i.e., a factor associated with signal and not noise) when the percentage of significance level of the F-test, %SL, is lower than a test level set in previous studies at 5% [28,29]. The ratio between the reduced eigenvalues, $R(r)$, which approaches one for noise factors, was also used in determining the number of factors. Once the number of individual components was set, XANES spectra corresponding to individual Pd or Cr species and their concentration versus temperature profiles were generated by an orthogonal rotation (varimax rotation), which should align factors (as closely as possible) along the unknown concentration profiles, followed by iterative transformation factor analysis (ITFA). ITFA starts with delta function representations of the concentration profiles, associated with each chemical species, located at temperatures predicted by the varimax rotation, which are then subjected to refinement by iteration until error in the resulting concentration profiles is lower than the statistical error extracted from the set of raw spectra [28–30].

3. Results

3.1. Activity results

The CO and NO conversion profiles for Pd and Pd–Cr catalysts containing 1 wt% of Cr are presented in Figs. 1A and 1B, respectively. A CrCZA reference system has also been included for comparison purposes. Below 350 K, conversion of NO corresponds to adsorption/desorption phenomena, as calculated by mass balance of the outlet gases. NO_2 was never detected after contact of the reaction mixture with the samples. Concerning N-selectivity of the reduction process, a maximum of N_2O of roughly 30% was obtained for all catalysts at temperatures below full conversion. For PdA, PdCZA, and PdxCrCZA full selectivity to N_2 is reached around 480–520 K, while Pd1CrA only gets to that point above 580 K. With the exception of PdA, CO oxidation over all samples proceeds at a lower temperature than NO reduction. A comparison of light-off behavior for all samples may be obtained by comparing the temperatures (Table 1) required to attain 50% conversion. As can be de-

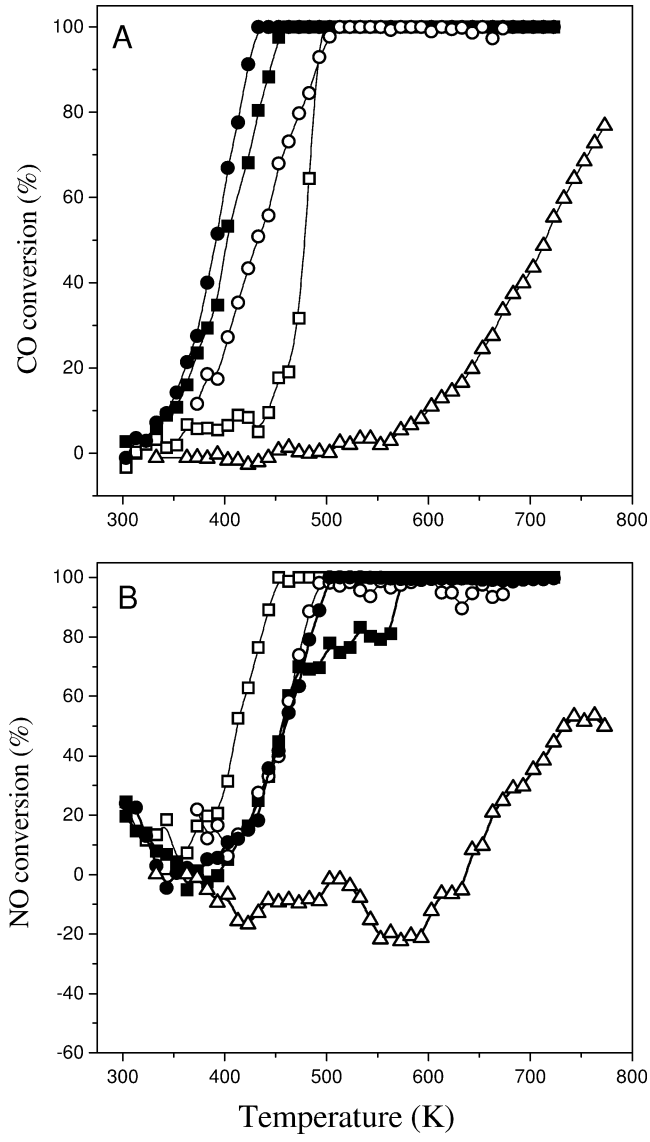

Fig. 1. CO (A) and NO (B) conversion profiles for the $CO + NO + O_2$ reaction over palladium–chromium (closed symbols) samples and monometallic references (open symbols). Circles, Pd1CrCZA and PdCZA; squares, Pd1CrA and PdA; triangles, CrCZA.

duced from Fig. 1 and Table 1, the temperature difference between the two reactions ranges from about 25 K for PdCZA to 75 K for Pd05CrCZA. The addition of Cr exhibits catalytic effects with a marked dependence on the support; in the case of alumina, it appears that Cr decreases the CO light-off by 75 K and increases the NO value by ca. 45 K. An additional effect is the existence of a plateau in NO conversion (Fig. 1B) at temperatures from ca. 450 to 550 K. A lesser effect, on the other hand, is observed for the CZA

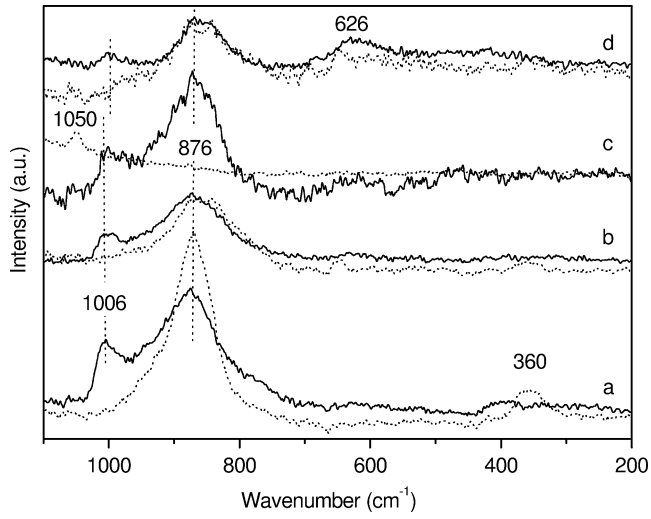

Fig. 2. Raman spectra of CrA (a), Pd1CrA (b), CrCZA (c), and Pd1CrCZA (d) samples. Dashed lines, hydrated samples; full lines, calcined samples.

supported samples, with a moderate decrease in CO light-off and negligible influence on NO reduction. In this case, Cr loading had only a slight influence on CO conversion and did not influence NO reduction performance. Cr-only catalysts display poor performance in both reactions, the best performance being achieved using CrCZA, Fig. 1.

3.2. Sample characterization

Calcined samples were analyzed using XRD, TEM-XEDS, Raman, and EPR spectroscopies. A summary of XRD/TEM results is presented in Table 2 and mainly reflects information concerning the ceria–zirconia (CZ) component; significant differences were not apparent from comparing the Cr-containing samples analyzed here and the monometallic Pd reference samples reported earlier [27]. Briefly, the CZ-supported component has a Ce:Zr atomic ratio of ~ 1, with an average crystallite size of 2 nm, and is irregularly dispersed over the alumina support [7]. CZ patches can be classified in two simple groups: bidimensional patches with strong interaction with alumina and tridimensional patches with properties approaching those of the bulk material [7,10]. In our case, bidimensional CZ entities are dominant [7].

Characterization of Cr and Pd in the oxidized state was performed using Raman and EPR spectroscopies. Mono and bimetallic systems containing 1 wt% of Cr have Raman spectra shown in Fig. 2. Spectra are shown for hydrated (as stored) and de-hydrated (calcined) samples; the strong changes observed between these states provide ev-

Table 1
50% isoconversion temperatures (T_{50}, K) observed for the bimetallic and monometallic reference catalysts in the $CO + O_2 + NO$ reaction at 30,000 h^{-1}

	Pd1CrCZA	Pd1CrA	Pd05CrCZA	Pd025CZA	PdCZA	PdA
T_{50} (CO conv.)	391	403	384	403	432	479
T_{50} (NO conv.)	458	458	458	458	455	412

Table 2
Summary of results for the ceria–zirconia component from XRD and TEM/ED/XEDS analysis

Sample	Cell parameter (Å)	Average particle size (nm)[a]	$(Ce/Zr)_{at.\ ratio}$[b]	$(Ce + Zr/Al)_{at.\ ratio}$[b,c]
PdCZA	5.30[d]	2	0.8–1.2	0.25–0.45
Pd1CrCZA	5.30[d]	2	0.8–1.3	0.2–0.5

[a] Obtained from dark-field TEM images using the (111) ring of $Ce_xZr_{1-x}O_2$.
[b] XEDS results.
[c] Only zones presenting detectable amounts of Ce,Zr are included.
[d] From electron diffraction results.

idence for the presence of highly dispersed species rather than well-developed Cr-containing phases [32–34]. The Raman profiles are dominated in all cases by bands at ca. 1005 and 875 cm^{-1}, ascribed to terminal Cr=O and bridging Cr–O–Cr vibrations, respectively, and attributed to Cr(VI) species in the form of chromates with different degrees of oligomerization [32–34]. These bands appear with diminished intensity in the presence of Pd. Additional minor bands are detected at 1050 cm^{-1} in the case of hydrated CrZCA, ascribed to the Cr=O stretch of isolated species [32–34], at 360 cm^{-1} for hydrated CrA, which can be attributed to a Cr–O deformation mode [32–34], and at 625 cm^{-1} for calcined Pd1CrCZA. The last is typical of alumina-supported Cr materials [32,34] and may be associated with the presence of amorphous or poorly crystalline Cr_2O_3. In connection with this band, it is interesting to note the absence of a sharp band close to 550 cm^{-1}due to crystalline Cr_2O_3 [32–34]. An alternative assignment of bands around 650 cm^{-1} is the B_{2g} mode of PdO, since this material has a resonance-enhanced Raman signal peaking at this energy [35]. However, as the band is centered at 625 cm^{-1} and the excitation line used here is 415 nm it is unlikely that a resonance enhanced signal should be detected.

EPR spectra of the samples (Fig. 3) show a common, fairly symmetrical signal at $g = 1.970$ and with $\Delta H_{pp} \approx$ 45 G, whose integrated intensity represents a number of spins equivalent to ca. 5.0, 1.1, 1.7, and 1.6 wt% of the entire chromium content of the samples for CrA, Pd1CrA, CrZCA, and Pd1CrZCA, respectively. Additionally, a broad and poorly defined signal (inset of Fig. 3) appears at low magnetic field. It shows the highest intensity for Pd1CrA, decreasing significantly for CrZCA and Pd1CrZCA and was almost absent for CrA. The main difference between both signals concerns their behavior towards recording temperature: while a roughly threefold decrease is produced in the intensity of the signal at $g = 1.970$, indicating that the corresponding paramagnetic species approximately follows the Curie law, the intensity of the low-magnetic field signal essentially does not change or undergoes a slight increase when the spectrum is recorded at RT. The behavior of the signal at $g = 1.970$ is typical of isolated Cr(V) square pyramidal species [36,37]. The influence of the recording temperature of the low-field signal, along with its relatively large linewidth, suggests that it corresponds to species coupled with Cr(III) or Cr(IV) immersed in a ferro- or antiferromagnetic phase [38]. The presence of a weak, narrow signal at $g = 4.3$ was also noted (see the inset in Fig. 3), whose intensity decreased with increasing recording temperature, and which most likely corresponds to residual Fe^{3+} impurities present in the alumina support material.

3.3. In situ XANES analysis

Factor analysis results at the Pd K-edge (Table 3) for Pd1CrCZA, Pd1CrA, PdCZA, and PdA obtained during a temperature-programmed run under CO + NO + O_2 are consistent with the existence of two different chemical

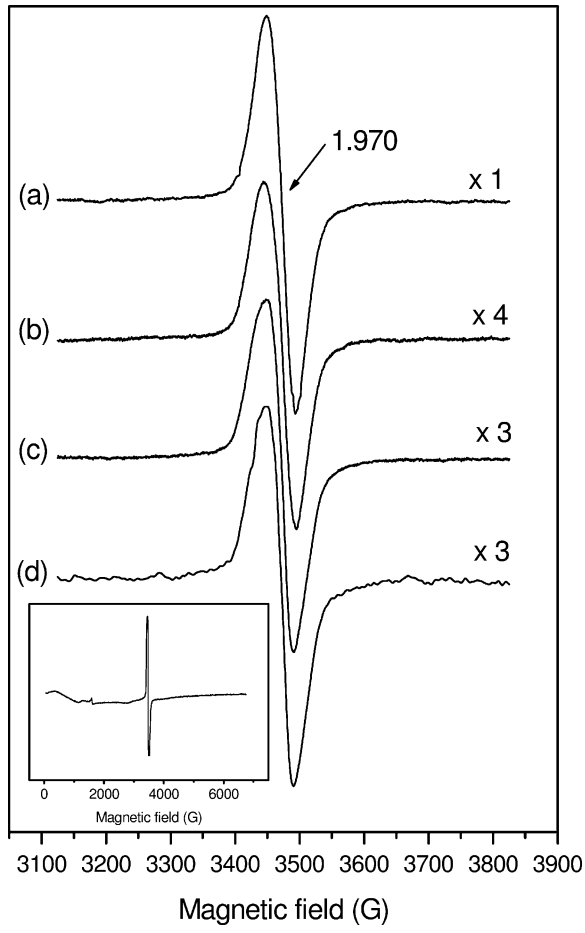

Fig. 3. EPR spectra at 77 K of CrA (a), Pd1CrA (b), CrCZA (c), and Pd1CrCZA (d). The inset shows a large magnetic field range spectrum of PdCrA.

Table 3
Principal component analysis of Pd K-edge XANES results

Factor	Eigenvalue	%SL	$R(r)$	Variance
		A. PdA		
1	491.351	0.00	701.23	99.868
2	0.64410	0.00	272.15	0.021
3	0.00217	8.03	2.08	0.001
4	0.00095	17.90	1.29	0.001
5	0.00066	20.61	1.46	
6	0.00041	27.85	1.13	
7	0.00032	29.84	1.33	
8	0.00021	37.27	1.03	
		B. Pd1CrA		
1	546.3	0.00	1104.32	99.914
2	0.45848	0.00	53.83	0.014
3	0.00779	0.07	13.04	0.002
4	0.00055	21.35	1.17	
5	0.00042	22.53	1.36	
6	0.00028	28.41	1.29	
7	0.00019	34.48	1.08	
8	0.00015	36.98	0.98	
		C. PdCZA		
1	458.49	0.00	1334.23	99.930
2	0.31594	0.00	194.34	0.070
3	0.00149	10.24	1.45	0.001
4	0.00092	12.38	2.06	0.001
5	0.00040	25.48	1.23	
6	0.00029	29.50	1.22	
7	0.00021	34.36	1.01	
8	0.00018	35.02	1.10	
		D. Pd1CrCZA		
1	762.732	0.00	1334.65	99.929
2	0.53430	0.00	135.34	0.070
3	0.00366	7.24	1.29	0.001
4	0.00261	5.87	2.34	
5	0.00102	16.84	1.88	
6	0.00048	30.13	1.15	
7	0.00038	33.46	0.98	
8	0.00036	33.07	1.08	

Variances lower than 10^{-3} are not reported.

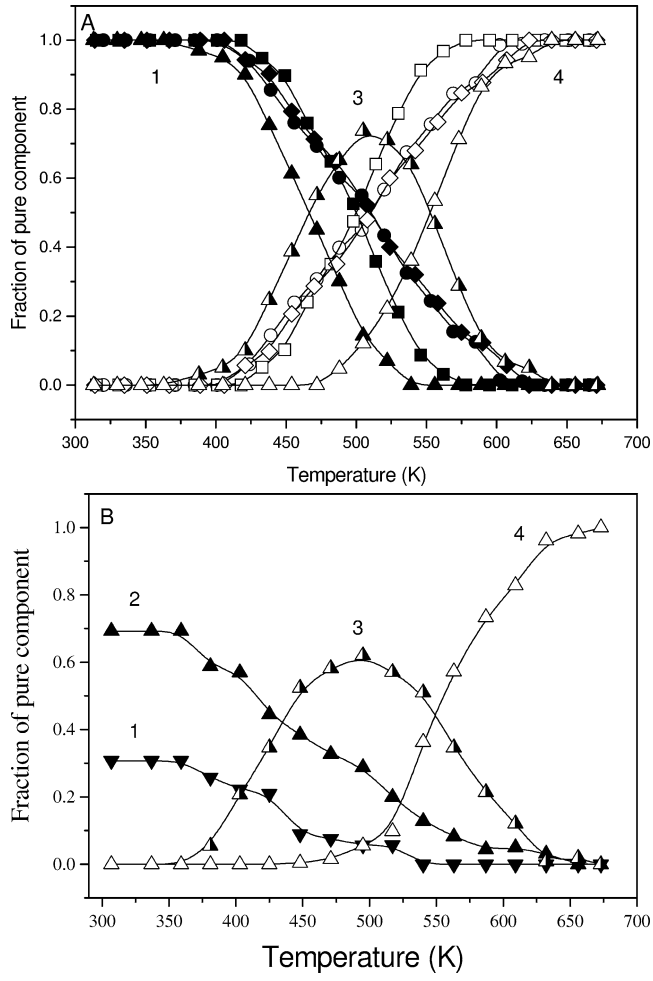

Fig. 4. Concentration profiles during the temperature-programmed reaction run for Pd- (A) and Cr-containing species (B). Initial species (filled symbols; species number 1 and 2); intermediate species (half-filled symbols; species number 3), and final species (open symbols; species number 4). Circles, Pd1CrCZA; rhombs, PdCZA; triangles, Pd1CrA; squares, PdA.

species except in the case of Pd1CrA, where three chemical species are detected. The number of species is clearly indicated by sharp variations in the % SL and $R(r)$ values displayed in Table 3. In Fig. 4A the fraction of these chemical species as a function of sample temperature are depicted. This plot shows that Pd is present initially as only one chemical form when the reaction starts. This compound is then directly converted to a final state in samples where only two species in total were detected, while for Pd1CrA, which showed evidence for three species, conversion from initial to final sates involved an intermediate species. The temperature at which the maximum rate of initial-state (chemical species) disappearance occurred was lower for Pd1CrA (ca. 450 K) but very similar for the other samples (ca. 490 K for PdA and 510 K for Pd1CrCZA and PdCZA). In all cases, only one Pd species was detected above 625 K.

When compared with the reference spectrum of PdO (Fig. 5A,a), the shape of the XANES spectrum of the samples in their oxidized state shows only slight differences which may be a consequence of the limited particle size of the oxidic Pd-containing entities. This suggests similar local symmetry (D_{2h}) and oxygen first-shell coordination distances among the samples and also in the PdO reference. Similarly, the XANES spectra of the final state detected in the reaction (Fig. 5B) do not display significant differences between samples and can be readily identified as zerovalent Pd. Slight differences when compared with the reference Pd foil (Fig. 5B,a) include the smaller intensity of the continuum resonances (CRs), particularly for Pd1CrCZA, and a shift to lower energy (ca. 1.4 eV; similar in all catalysts) for the $4f$ CR (located around 24,390 eV). As Pd–Cr alloys have reduced fcc lattice parameters with respect to Pd [39] and the positions of CRs have an inverse dependence with the square of the coordination distance, the formation of such a binary phase would be consistent with a shift to higher energies, as occurs with the Pd L_{III}-edge White line [40]. It appears that

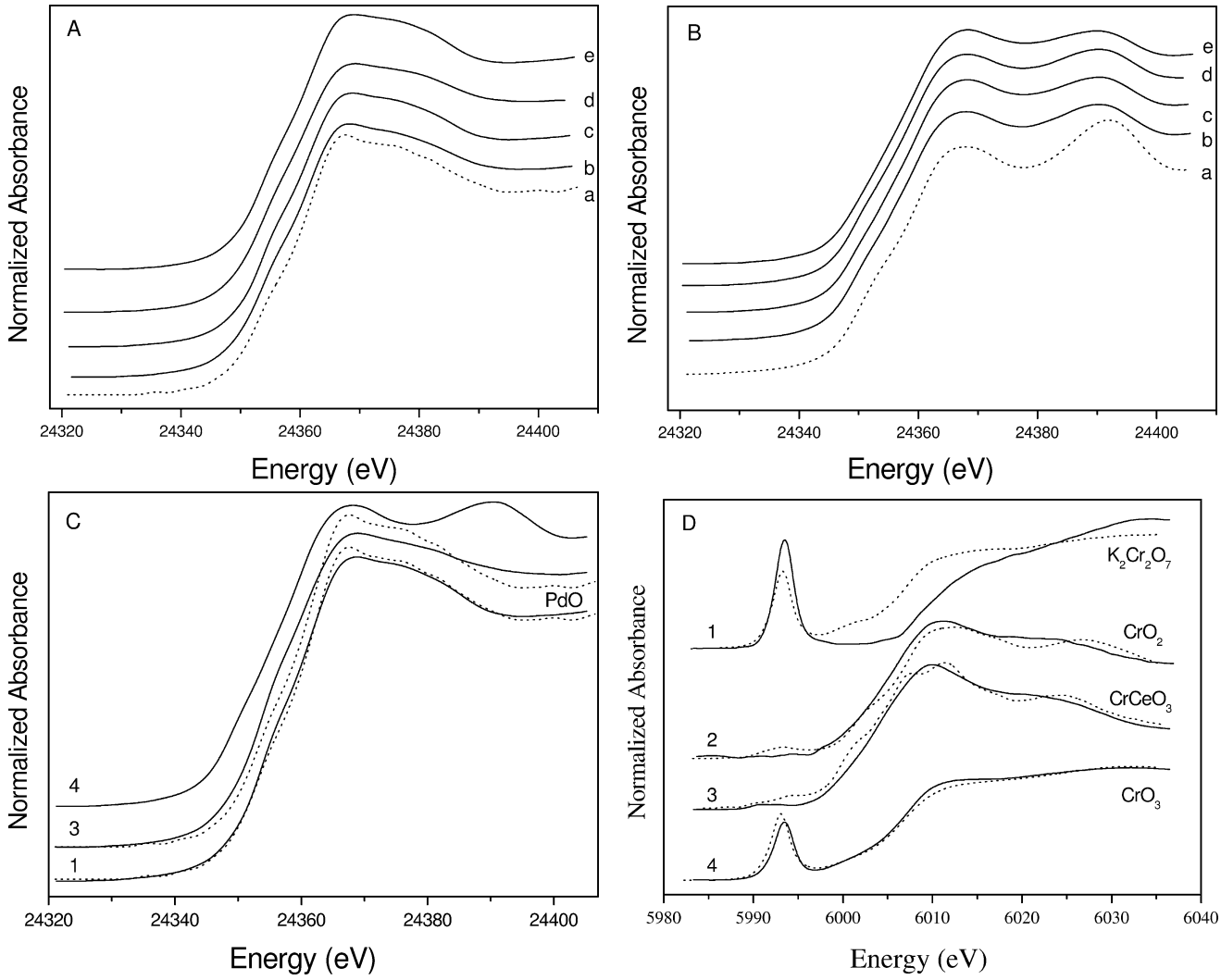

Fig. 5. XANES spectra for PCA predicted chemical species. (A) Pd initial, oxidized species; (B) Pd final, reduced species; (C) Pd species detected for the Pd1CrA sample; and (D) Cr species detected for the Pd1CrA sample. Lower case labels: (a) reference compounds, PdO or Pd; (b) PdA; (c) Pd1CrA; (d) PdCZA, (e) Pd1CrCZA. Labels 1 to 4 as in Fig. 4.

the presence of Cr in the Pd network must be limited at most to a small percentage and that differences with the reference foil mostly reflects the small particle size and/or an interaction with the support component (particularly with the CZA support). The XANES spectrum of the intermediate compound detected for Pd1CrA is presented in Fig. 5C together with the spectra of the other two Pd-containing species and the PdO reference. Although its shape is rather complex to interpret in detail, the edge position (which is located at lower energy than the shoulder d-like resonance observed at the adsorption edge region) indicates a Pd(I)-like partially reduced state. This interpretation is based upon the universal linear relationship that has been shown to exist between the formal oxidation state and the edge or CR position (see, for example, Ref. [30]). The presence of a Pd partially reduced state is further confirmed by the decreasing intensity (with respect to the calcined material species numbered as 1 in Fig. 5C) of the first ($5sp$) CR located ca. 24,365 eV.

Further information concerning the chemical nature of the intermediate was obtained by studying the Cr K-edge of the Pd1CrA (and CrA) sample(s). In this case, Table 4 gives evidence for the existence of four species. Fig. 4B shows the presence of two initial species in Pd1CrA, which

Table 4
Principal component analysis of Cr K-edge XANES results for Pd1CrA

Factor	Eigenvalue	%SL	$R(r)$	Variance
		Pd1CrA		
1	851.332	0.00	285.33	99.674
2	2.64623	0.00	193.15	0.323
3	0.01261	0.82	2.22	0.002
4	0.00521	0.63	4.06	0.001
5	0.00117	7.07	3.00	
6	0.00035	25.88	1.46	
7	0.00021	34.90	0.93	
8	0.00020	33.33	1.08	

Variances lower than 10^{-3} are not reported.

are converted to an intermediate state above ca. 350 K, giving another, final state above ca. 520 K. Consistent with results at the Pd *K*-edge, transformation of the Cr species was complete by 625 K. In Fig. 5D, the corresponding XANES spectra of the Cr species are presented along with some reference compounds. Comparison of the $1s \rightarrow 3d$ pre-edge feature (located around 5995 eV) and edge shape indicates the chemical nature of the two species present when the Pd1CrA was initially exposed to the reaction mixture; a non-centrosymmetric tetrahedral or subgroup Cr(VI) compound, with some similarities to the distorted-tetrahedral $K_2Cr_2O_7$ reference, and another one similar to Cr(IV) in an oxidic environment. The presence of both Cr chemical states for alumina-supported materials calcined above 573 K has been shown on the basis of spectroscopic characterization studies [32–34,41,42]. It can be noted, however, that, according to the XANES data, the sample here seems to contain predominantly Cr(VI) after calcination (result not shown). The main point to stress here is that an intermediate compound with maximum concentration about ca. 520 K is also observed at the Cr *K*-edge. Comparison with reference materials suggests that the compound contains Cr(III). Note that the huge edge shift (ca. 2–3 eV) displayed between Cr formal oxidation states differing in one unit is extremely useful in providing an accurate description of the oxidation state [30,41]. As this intermediate evolves with temperature, a Cr(VI) state in an oxidic environment (CrO_3-like) is recovered. The CrA reference, on the other hand, also displays the presence of a CrO_3-like species in the calcined state, in this case showing stability throughout the temperature ramp under the reactive atmosphere.

3.4. In situ DRIFTS

Spectra recorded under the $CO + NO + O_2$ mixture for PdA, Pd1CrA, PdCZA, and Pd1CrCZA samples are shown in Figs. 6A–6D, respectively. A rough correlation can be observed for all samples between evolution of bands due to gaseous CO (barely discernible doublet in the 2200–2050 cm^{-1} region) and CO_2 (2400–2300 cm^{-1}) and the CO conversion profiles (Fig. 1A). In general, the spectra give evidence for the presence of different carbonyl species mainly adsorbed onto Pd. Cr carbonyl contributions, which may be detected around 2160–2170 cm^{-1} [43], are not observed, even for the CrCZA reference catalyst (result not shown). This may be attributed to the low adsorption enthalpy of CO on Cr [43]. Analysis of Pd carbonyls is made on the basis of previous results for the monometallic references [27,44,45].

At low temperatures, a shoulder (above the CO gas contribution) located at or below 2100 cm^{-1}, and a broad band centered around 1980–1970 cm^{-1} were observed for all Pd-containing samples (Figs. 6A–6D). The former, which displays a significant red shift with temperature, was observed down to ca. 2050 cm^{-1} and is attributed to CO adsorbed onto Pd(0) on-top sites [27,43,44,46]. The lower-frequency band, which also shows a red shift with increasing temperature, is assigned to bridging carbonyl species adsorbed onto Pd(0) [27,44–46]. For both carbonyl species, the red shifts observed result from a continuous decrease in CO coverage of Pd particles resulting either from desorption or from reaction with oxygen at these centers. The magnitude of the shift may reflect differences between the relative adsorption enthalpies of CO on these sites [46], between adsorbed molecule distances and/or between different catalytic activities for such centers. The observed shift was greater for the linearly adsorbed species.

As a general rule, the intensity of carbonyls adsorbed onto Pd(0) sites was decreased in the presence of Cr. An additional band at 2155–2158 cm^{-1} assigned to CO adsorbed onto Pd(II) sites [27,44–47] was detected in all cases except PdA. In the case of PdA and less so for the other samples, a band at ca. 2120–2130 cm^{-1}, also related to the presence of surface Pd(II) [25,44–47], was observed. The temperature dependence of the adsorbed Pd(II) carbonyl species was very similar among the samples studied. DRIFTS spectra also contained bands at 2250 and 2232 cm^{-1}, which were not detected in the absence of NO in the reactive mixture [7,21,27], and can be ascribed to isocyanate species adsorbed at octahedral and tetrahedral Al^{3+} cations, respectively [48]. This species results from NO decomposition followed by N–CO combination on metal particles and spillover onto support sites, and the large intensity of the ν_{as}NCO band and thus its ease of detection may be used to roughly determine the onset temperature for NO dissociation [42–48].

To examine the state of the metal surfaces on completion of the reaction runs and in the absence of thermally driven adsorption effects, samples were flushed at 623 K, cooled in N_2 to room temperature, and subsequently exposed to 1% CO/N_2 before the cell was again flushed with N_2. Spectra recorded during this treatment are displayed in Fig. 7. A band centred at 1990–1980 cm^{-1}, present in all samples and attributed to bridging carbonyls adsorbed onto metallic Pd particles, was observed with attenuated intensity for the CZA-supported samples. The presence of Cr also affected the intensity of the latter, but this was more marked for the alumina-supported samples. As a shoulder on the band due to bridging carbonyls, a broad band centered ca. 1925 cm^{-1} was observed for PdA and with very small intensity for the remaining samples and attributed to CO adsorbed in three-fold hollow sites on Pd(0) [27,44–47]. Linear Pd(0) carbonyls (band ca. 2095–2100 cm^{-1}) were detected for the monometallic references, with greater intensity for PdCZA, but were almost absent in the presence of Cr. This linear carbonyl was the most affected by the purging step in accordance with its low adsorption enthalpy. Additional bands at 2118–2124 and 2152 cm^{-1} can be attributed to adsorption onto Pd(I) and Pd(II), respectively [21,22,27,44–47]. It should be mentioned, however, that the presence of Cr carbonyls cannot be excluded in the presence of CO gas, although

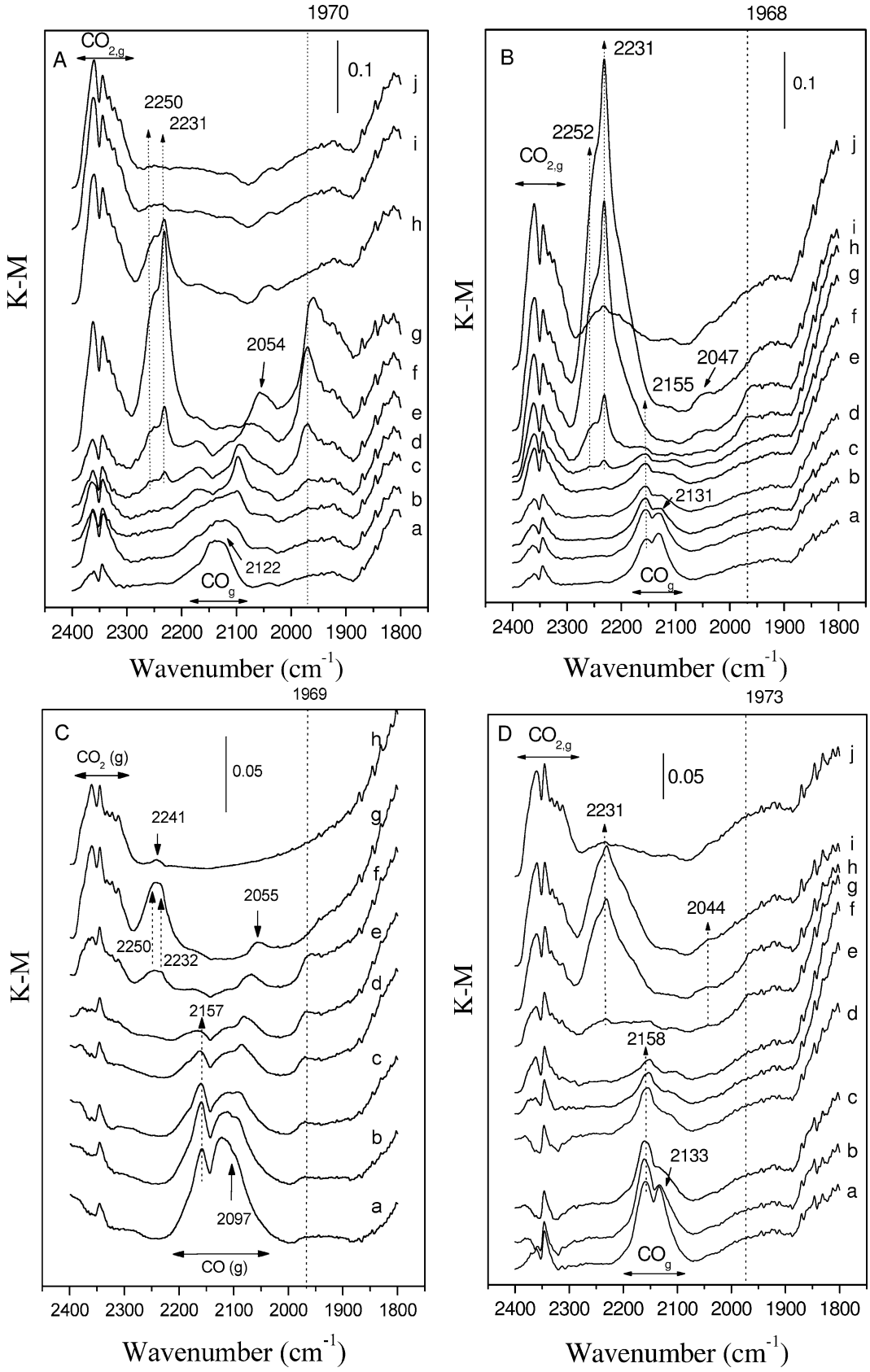

Fig. 6. DRIFTS spectra of (A) PdA, (B) Pd1CrA, (C) PdCZA, and (D) Pd1CrCZA samples in a flow of 1% CO, 0.45% O_2, 0.1% NO, N_2 balance at (a) 303, (b) 333, (c) 363, (d) 393, (e) 423, (f) 453, (g) 483, (h) 513, (i) 543, and (j) 573 K.

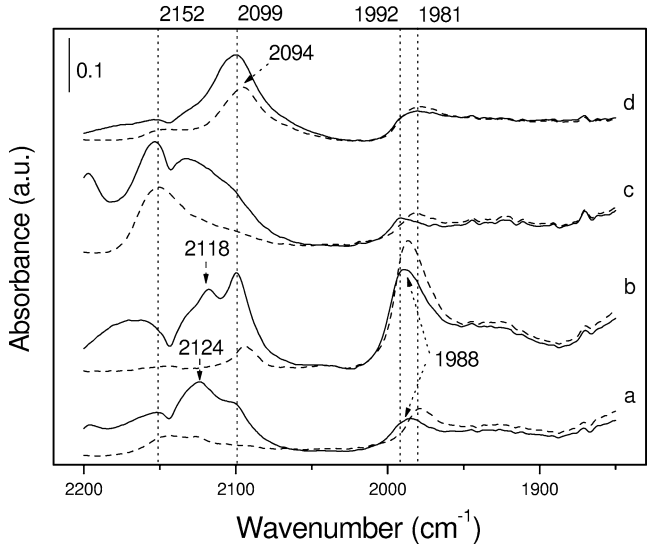

Fig. 7. DRIFTS spectra following experiments shown in Fig. 6 after exposure to CO (full lines) and subsequent flushing with N_2 (dashed lines). (a) Pd1CrA, (b) PdA, (c) Pd1CrCZA, and (d) PdCZA.

their absence was noted in the CrCZA case. Results in Fig. 7 give firsthand evidence that the Pd morphology/particle size is very different for A and CZA monometallic samples. This is supported by the intensity ratio of the on-top to bridge Pd(0) carbonyl bands. On the other hand, Cr has two clear effects. First, in A-supported specimens a drastic influence on morphology is shown by the strong decrease in Pd(0) bridging carbonyls. This can be mainly related (as described below) to the genesis step of the Pd zerovalent phase. Second, the intensity of bands related to oxidized Pd centers clearly indicates that the presence of Cr favors the formation of such centers, at the surface, independent of the nature of the support. This appears to selectively influence the Pd, centers where CO is adsorbed in the ontop mode and located in closed packed (111)-like planes, having much lesser impact in those corresponding to open (100)-like planes which are mainly (although not exclusively) associated with the CO bridging adsorption mode [21,22, 27,44–47,49]. Of course, the analysis of the second effect is somewhat masked by the first in the case of the alumina-supported samples.

4. Discussion

4.1. Structural and morphological nature of samples

As is evident from Section 3, a clear influence of the support on the evolution of samples with temperature is observed under reaction conditions. In the case of alumina-supported samples, a degree of interaction between the noble metal and the Cr is apparent, even in the calcined material. This is schematically represented in Fig. 8I A, where according to XANES, both metals are mainly inserted into oxidic matrixes with Pd(II) (PdO-like) and Cr(VI) (CrO_3-like) oxidation states. The EPR spectra show that the Cr EPR-visible species are influenced by the presence of the Pd, decreasing the amount of Cr(V) and indicating the presence of a phase containing magnetically coupled cations in the Pd1CrA catalyst but not present for CrA. This influence is also evident in the evolution of the XANES Cr *K*-edge spectra immediately upon contact with the reactive mixture at RT; as depicted in Fig. 8I B and justified by the XANES study, the reaction mixture changes the Cr phase distribution and chemical state, giving a tetrahedral Cr(VI) plus a Cr(IV), CrO_2-like chemical phase. For the sake for simplicity, Fig. 8I does not differentiate between the two Cr(VI) phases already mentioned. Although the extent and nature of the Pd–Cr interaction is unclear, both techniques do show that Pd and Cr are in sufficiently close proximity to alter the behavior of the Pd1CrA system significantly with respect to the monometallic reference. The close proximity of both active elements in the calcined state induces the formation of an intermediate in the ca. 350–625 K temperature range (Fig. 8I C), this phase containing Pd(I) and Cr(III) as the principal oxidation states and, in terms of its local order, showing similarity to $PdCrO_2$ oxide [25]. This chemical compound has Pd–Pd distances of 2.83 Å, very close to metallic dimensions (2.75 Å), giving a 1-D (dimension) electronic conductor [25], with some Pd5*s* electron delocalization, resembling the metal.

Around 520 K this binary oxide is transformed, yielding two monometallic single phases containing Pd(0) and Cr(VI) (Fig. 8I.D). It should be stressed that the evolution of this chemical compound gives the same Pd and Cr phases as the monometallic references at temperatures above 520 K. No evidence is detected that would indicate the formation of a binary Pd–Cr alloy, in spite of the existence of the binary oxidic precursor. The presence of a miscibility gap for bulk Pd–Cr alloys has been reported, and typically a maximum of ca. 15 at% Cr is known to be substitutionally present in the fcc lattice structure of Pd [26,39]. The absence of a significant alloying effect for samples here indicates that the Pd–Cr bulk alloy binary phase diagram obtained for bulk phases [26] is also appropriate for nanosized materials and that the surface contribution to the total energy may further lower the limit of Cr solubility in the Pd. An additional influence of the gas phase on the resulting zerovalent phase composition may also need to be considered. In any case, it is clear that Pd–Cr alloy phases have been described under (CO + NO) stoichiometric mixtures only in prereduced (H_2 at 870 K) materials [19], indicating that the presence of Cr(0) before and/or at the beginning of the reaction may be of importance in obtaining/maintaining the binary zerovalent phase. The formation of metallic Pd particles from the Pd–Cr oxidic intermediate has, however, a clear impact on the final zerovalent Pd phases formed. Comparison of IR results for CO-adsorption on postreaction samples mainly shows a lowering of the bridge and threefold Pd(0) carbonyls as well as a larger intensity of Pd(II) in the presence of Cr. The first fact clearly indicates a smaller

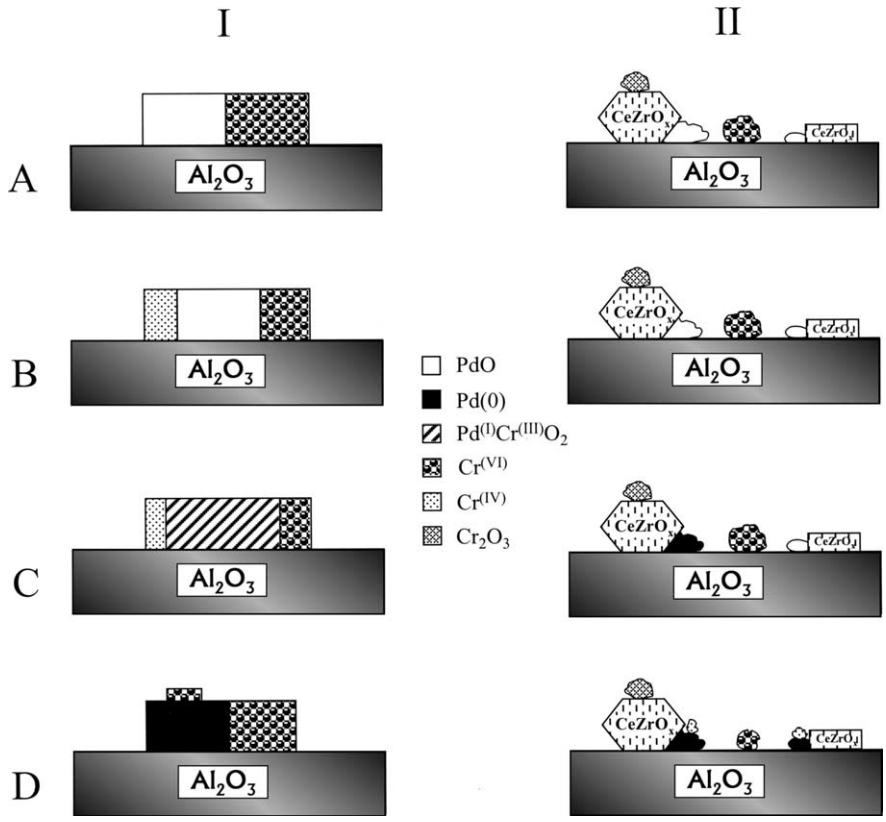

Fig. 8. Schematic view of the main Pd- and Cr-containing chemical phases detected in the Pd1CrA (I) and Pd1CrCZA (II) systems. (A) sketch visualizes the calcined materials; (B), (C), and (D) sketches of systems under the reaction mixture at temperatures below 400 K, at 500 K, and above the latter.

particle size of the monometallic Pd particles, while the second gives evidence for the coexistence of metallic and oxidized Pd sites at the surface, which may be driven by the presence at the high (reaction) temperatures of small oxidic Cr entities (ions or small aggregates) at the surface of the noble metal particles. The presence of such oxidized entities has been also mentioned for Mn or Mo (Pd-) bimetallic catalysts [16–18].

In the case of CZA-supported samples, there was no evidence from EPR, Raman, or XANES for any significant interaction between Pd, either in the oxidized, Pd(II), or partially reduced, Pd(I), state, and Cr. This absence of interaction between the components was found for Pd–Cr catalysts with Pd:Cr atomic ratios from 0.5 to 2. It seems that the presence of the CZ component prevents, to a large extent, the close proximity of these components in these novel ceria–zirconia TWC catalysts. As Raman spectra (Fig. 2) suggest broadly similar Cr distributions on A and CZA after calcination, the absence of Cr–Pd interactions could be attributed to the Pd distribution, which tends to locate Pd at the interface between the CZ patches and the A carrier in the CZA-supported sample [27]. This is schematically shown in Fig. 8II A, where Pd particles are located at the mentioned interface between CZ patches and alumina, and Cr entities can be present in both the alumina carrier, as Cr(VI) oligomers, and CZ patches, as amorphous or poorly crystalline Cr_2O_3-like entities (which, according to Raman results, is the Cr species exclusive of CZA materials). This Pd1CrCZA system does not evolve until the reaction temperature exceeds 400 K (Figs. 8II B and C). The Pd zerovalent particles formed are not significantly affected in terms of either their size or morphological characteristics by the presence of Cr, although the surfaces of these particles display a significant quantity of Pd(II) sites after reaction. Again, this suggests the presence of small Cr ions or aggregates located at the surface of the noble metal particles (Fig. 8II D). The Pd(II)/Pd(0) surface equilibrium is shifted to the oxidized state to a greater extent for CZA- than for A-supported Cr-containing materials, but this effect may also be observed for the monometallic Pd references (Fig. 7) and has been previously reported for such reference Pd samples [44].

4.2. CO oxidation and NO reduction

In Table 5 IR and XANES evidence for the onset temperatures of reduced Pd (Pd(0) and Pd(I)) state formation has been summarized and the results compared with the initial (T_0) and T_{50} temperatures corresponding to 50% conversion of CO or NO. Note, of course, that T_{IR} values in Table 5, which point to the presence of surface Pd(0) entities, are subject to CO_g availability and, thus, depend on CO conversion level. For NO reduction, catalytic activity data are shown only for the 50% conversion level, as the onset

Table 5
Onset temperatures for IR detection of NCO (T_{NCO}, K) and Pd(0) carbonyls (T_{IR}, K) and for detection of Pd(I) and Pd(0) by XANES (T_{XANES}, K) and initial and 50% conversion temperatures (T_0 or T_{50}, K) for PdA, Pd1CrA, PdCZA, and Pd1CrCZA samples

Samples	Pd(0) (Pd(I)) onset		T_0, T_{50} CO	T_{NCO}	T_{50}, NO
	T_{IR}	T_{XANES}			
PdA	363	420	350, 479	423	412
Pd1CrA	423	470 (350)	321, 403	453	458
PdCZA	363	410	352, 432	453	458
Pd1CrCZA	423	410	321, 391	483	458

is not readily discernible due to the adsorption–desorption phenomena at low temperatures and, in any case, differences at the onset of the light-off are roughly equivalent at higher levels of conversion.

The behavior of PdA for CO oxidation is consistent with a Langmuir–Hinshelwood mechanism, as observed for model Pd/SiO_2 systems [46]. In the model case mentioned, at temperatures below initial light-off CO coverage of the metallic Pd particles is close to unity and the rate-determining step is the rate of creation of vacant sites by desorption of CO, where oxidants (NO/O_2) can be activated [46]. Although this model has widespread applicability, Hoffman et al. [49] have recently shown that the CO-poisoning effect of the metal surface is strongly diminished for small particles. For preoxidized materials (such as those used here), the catalytic activity is very low until extensive reduction of Pd by CO can take place [27,44,45] and a rough correlation can be established for PdA between the temperature of appearance of Pd(0) sites at the surface by DRIFTS, when NO is used as oxidant and the corresponding temperature of appearance of bulk Pd(0) by XANES when oxygen is used (Table 5). In the case of the alumina-supported system, the preference of CO for NO or O_2 as oxidant depends to a large extent on the Pd particle size which, in turn, drives the type (open vs closed and number of edge and steps) of surface exposed to the reactants, and is mainly based on the fact that NO dissociation and reduction are structure-sensitive processes which are favored in systems with large particle size [44–47].

The presence of Cr in the A-supported catalysts dramatically decreases the temperature for CO oxidation. In this case, the correlation is with the presence of the Pd(I)–Cr(III) phase (Table 5). This is likely due to the metallic-like character of the Pd 5*sp* band, which is still able to activate the CO molecule and to initiate the reaction. In this case, the absence (or further decrease) of the CO-poisoning effect (characteristic of the noble, zerovalent phase) can be also claimed to contribute to the reduction in light-off temperature. Note, on the other hand, that classical Pd(I) and Pd(II) states (in their monometallic oxide form) are usually believed to be less effective for CO oxidation that metallic-like states [26,27,44, 45,50].

It is well known that the presence of a reducible oxide such as CZ decreases the CO oxidation light-off temperature with respect to alumina-supported catalysts due to the existence of a Pd–CZ interaction where additional sites for oxidant (NO/O_2) activation are readily generated [27,44,51] and, in some cases, by the ease with which metallic Pd is formed [44]. Here, the presence of Cr plays only a secondary role, decreasing the light-off temperature by less than half of what is detected for the alumina system. As only small changes in particle size are expected on going from PdCZA to Pd1CrCZA (DRIFTS results in Fig. 7), the effect of this parameter on light-off performance can be eliminated. A more likely explanation can be proposed by considering that the Pd(II)/Pd(0) surface distribution shows more bias toward oxidized states in the presence of Cr. This would suggest enhanced NO and/or O_2 dissociation assisted by the Pd–Cr interface, which would lead to a reduced CO coverage of the metallic particles and, consequently, to a reduction of the CO inhibition effect on light-off with respect to the alumina-supported samples.

With regards to NO reduction, Table 5 displays a rough correlation between the appearance of NCO and the T_{50}, NO temperature, indicating that this molecule can be used as a simple probe for the initiation of the NO reduction process. For this reaction, the introduction of Cr into the catalyst has detrimental effects on A-supported systems. A correlation can be established between the evolution of the Pd(I)–Cr(III) intermediate concentration (Fig. 4) and NO conversion (Fig. 1A), particularly for the plateau detected in the conversion plot (450–550 K) and the region of maximum concentration of the intermediate. It therefore appears that the lower performance of the palladium alumina-supported in the presence of Cr can be ascribed to a lower activity of the Pd(I)–Cr(III) intermediate for NO activation (always with respect to the metallic, Pd reference). In fact, small variations in the Pd valence density of metallic-like systems have either no effect or a moderate influence on CO activation, while the corresponding NO process can be strongly favored or hindered [52]. Moreover, the interaction between Pd and Cr_2O_3 appears to have little impact on the CO desorption temperature and C–O stretching frequency of such molecules when adsorbed onto the noble metal [53]. After the disappearance of the Pd(I)–Cr(III) and in the presence of Pd(0) the NO conversion profile reaches 100%.

For CZA-supported materials, no significant influence of Cr is detected. This despite the clear enhancement in NO (and/or O_2) dissociation already mentioned on the basis of the IR results and attributed to the presence of Cr entities at the Pd surface. Although these observations are not easily reconciled, they might be rationalized by suggesting an influence of Cr species on the N-coupling step(s) of the reduction process. Whether such step occurs near or at the Pd–CZ interface and/or is modified directly by Cr presence at such sites or indirectly through modification of interfacial Ce (or Zr) centers remains unknown. Additionally, comparison with PdA indicates that the Pd–CZ interface does not appear to promote this reaction in our system, contrarily to previous literature reports for similar reactions [43,54]. However, a comparison between PdA and PdCZA must be affected by

particle size effects (Fig. 7), which exert a very important influence on the NO dissociation process [44–47]. The Pd size distribution and interaction with the support is known to favor NO reduction in suitably prepared alumina systems with respect to ceria or ceria–zirconia promoted catalysts [55].

5. Conclusions

The behavior of a series of Pd–Cr bimetallic catalysts in CO oxidation and NO reduction processes has been tested and compared with that of monometallic Pd references. The catalytic properties display strongly dependence on the degree of interaction existing between both metals in the calcined state and this is in turn dependent on the nature of the support.

In the case of alumina, both metals are closely located following calcination. Under reaction conditions, this proximity induces the formation at low or intermediate temperatures of a Pd(I)–Cr(III) mixed oxide phase which alters the catalytic response with respect to the monometallic Pd reference. This phase is apparently capable of activating CO and its presence at lower temperatures than zerovalent Pd in the reference system significantly reduces CO light-off temperature. In contrast, this phase is detrimental for NO reduction. It appears that such a Pd–Cr mixed oxide could be used to enhance Pd activity in oxidation reactions. For $(Ce,Zr)O_x/Al_2O_3$ supported systems, no evidence was found of significant interactions between the metals in the calcined state in a series of catalysts with Pd:Cr atomic ratios ranging from 0.5 to 2. However, under the course of the reaction, formation of Pd(0) particles with Cr entities at the surface was detected at high temperature. This may enhance NO activation/dissociation and moderately favor CO oxidation but does not have any effect on NO reduction. This could be rationalized by considering that Cr may affect N-coupling steps.

Acknowledgments

We thank the Comunidad de Madrid for grants received (to A.B.H. and A.I.-J.), with which this work has been carried out, and for financial assistance (to A.B.H.) under the "Ayudas para estancias breves en centros de investigación extranjeros" program. We are also grateful to the scientific and technical staff at Daresbury SRS (beam time Ref. 38285) and the ESRF Synchrotron (BM29) for their help during the XANES experiments, to Mr. F. Sánchez for EPR measurements, and to Dr. M.A. Bañares for recording Raman data. Financial help by CICYT (Project MAT2000-1467) is also acknowledged.

References

[1] E.S.J. Lox, B.H. Engler, in: G. Ertl, H. Knözinger, J. Weitkamp (Eds.), Environmental Catalysis, Wiley–VCH, 1999, p. 1.
[2] A. Trovarelli, Catal. Rev. Sci. Eng. 38 (1996) 97, and references therein.
[3] D.S. Lafyatis, G.P. Ansell, S.C. Bennett, J.C. Frost, P.J. Millington, R.R. Rajaram, A.P. Walker, T.H. Ballinger, Appl. Catal. B 18 (1998) 123.
[4] J. Kašpar, P. Fornasiero, M. Graziani, Catal. Today 50 (1999) 351.
[5] Y. Nagai, T. Yamamoto, T. Tanaka, S. Yoshida, T. Nonaka, T. Okamoto, A. Suda, M. Sugira, Catal. Today 74 (2002) 225.
[6] A. Martínez-Arias, M. Fernández-García, V. Ballesteros, L.N. Salamanca, C. Otero, J.C. Conesa, J. Soria, Langmuir 15 (1999) 4796.
[7] M. Fernández-García, A. Martínez-Arias, A. Iglesias-Juez, C. Belver, A.B. Hungría, J.C. Conesa, J. Soria, J. Catal. 194 (2000) 385.
[8] M.H. Yao, N.J. Blaird, F.W. Kunz, J. Catal. 166 (1997) 67.
[9] M. Ozawa, K. Matuda, S. Suzuki, J. Alloys Comp. 303–304 (2000) 56.
[10] M. Fernández-García, A. Martínez-Arias, A. Iglesias-Juez, C. Belver, A.B. Hungría, J.C. Conesa, J. Soria, Phys. Chem. Chem. Phys. 4 (2002) 2473–2481.
[11] R. van Yperen, D. Lindner, L. Mubmann, E.S. Lox, T. Kreuzer, Stud. Surf. Sci. Catal. 116 (1998) 51.
[12] Z. Hu, C.Z. Wan, Y.K. Lui, J. Dettling, J.J. Steger, Catal. Today 30 (1996) 83.
[13] M. Skoglundh, H. Johansson, L. Löwendahl, K. Jansson, L. Dahl, B. Hirschauer, Appl. Catal. B 7 (1996) 299.
[14] K.C. Taylor, Catal. Rev. Sci. Eng. 35 (1993) 457.
[15] B. Coq, F. Figueras, J. Mol. Catal. A 173 (2001) 117.
[16] T.E. Hoost, G.W. Graham, M. Shelef, O. Alexeev, B.C. Gates, Catal. Lett. 38 (1996) 57.
[17] M. Schmal, M.A.S. Baldanza, M.A. Vannice, J. Catal. 185 (1999) 138.
[18] J.F. Trillat, J. Massadier, B. Morawek, H. Praliaud, A.J. Renouprez, Stud. Surf. Sci. Catal. 116 (1998) 103.
[19] A. El Hamdaoui, G. Bergeret, J. Massadier, M. Primet, A.J. Renouprez, J. Catal. 148 (1994) 47.
[20] M. Fernández-García, A. Martínez-Arias, C. Belver, J.A. Anderson, J.C. Conesa, J. Soria, J. Catal. 190 (2000) 387.
[21] M. Fernández-García, A. Martínez-Arias, J.A. Anderson, J.C. Conesa, J. Soria, Stud. Surf. Sci. Catal. 130 (2000) 1325.
[22] A.B. Hungría, A. Iglesias-Juez, A. Martínez-Arias, M. Fernández-García, J.A. Anderson, J.C. Conesa, J. Soria, J. Catal. 206 (2002) 281.
[23] M. Fernández-García, J.C. Conesa, A. Clotet, J.M. Ricart, N. López, F. Illas, J. Phys. Chem. B 102 (1998) 141.
[24] M. Fernández-García, J.A. Anderson, G.L. Haller, J. Phys. Chem. 100 (1996) 16247.
[25] R.D. Shannon, D.B. Rogers, C.T. Prewitt, Inorg. Chem. 10 (1971) 713.
[26] T.B. Massalki, Binary Alloy Phase Diagram, Vol. 1, 2nd ed., ASM International, 1993.
[27] M. Fernández-García, A. Martínez-Arias, A. Iglesias-Juez, A.B. Hungría, J.A. Anderson, J.C. Conesa, J. Soria, Appl. Catal. B 31 (2001) 39.
[28] M. Fernández-García, C. Márquez-Alvarez, G.L. Haller, J. Phys. Chem. 99 (1995) 12565.
[29] C. Márquez-Alvarez, I. Rodríguez-Ramos, A. Guerrero-Ruiz, G.L. Haller, M. Fernández-García, J. Am. Chem. Soc. 119 (1997) 2905.
[30] M. Fernández-García, Catal. Rev. Sci. Eng. 44 (2002) 59.
[31] E.R. Malinowsky, Factor Analysis in Chemistry, Wiley, New York, 1991.
[32] M.I. Zaki, N.E. Foudad, J. Leyrer, H. Knozinger, Appl. Catal. 21 (1986) 359.
[33] B.M. Weckhuysen, I.E. Wachs, J. Phys. Chem. B 101 (1997) 2793.
[34] B. Grzybowska, J. Sloczynski, R. Grabowski, K. Wcislo, A. Kozlowska, J. Stoch, J. Zielinski, J. Catal. 178 (1998) 687.
[35] J.R. McBridge, K.C. Kass, W.H. Weber, Phys. Rev. B 44 (1991) 5016.
[36] D. Cordishi, M.C. Campa, V. Indovina, M. Occhiozzi, J. Chem. Soc. Faraday Trans. 90 (1994) 207.

[37] Z. Zhu, M. Hartmann, E.M. Maes, R.S. Czernuszevich, L. Kevan, J. Phys. Chem. B 104 (2000) 4690.
[38] O.F. Gorriz, L.E. Cadús, Appl. Catal. A 180 (1999) 247.
[39] D. Wang, J.D. Cleway, T.B. Flanegan, J. Alloys. Comp. 325 (2000) 151.
[40] Y.S. Lee, K.Y. Lim, C.N. Whang, Y. Jeon, Appl. Phys. A 70 (2000) 59.
[41] A. Ellison, G. Diakun, P. Worthington, J. Mol. Catal. 46 (1988) 131.
[42] P.G. Harrison, W. Daniell, Chem. Mater. 13 (2001) 1708, and references therein.
[43] M. Pykavy, V. Staemmler, O. Seiferth, H.J. Freund, Surf. Sci. 479 (2001) 11, and references therein.
[44] A. Martínez-Arias, M. Fernández-García, A. Iglesias-Juez, A.B. Hungría, J.A. Anderson, J.C. Conesa, J. Soria, Appl. Catal. B 31 (2001) 51.
[45] M. Fernández-García, A. Martínez-Arias, L.N. Salamanca, J.M. Coronado, J.A. Anderson, J.C. Conesa, J. Soria, J. Catal. 187 (1999) 474.
[46] X. Xu, D.W. Goodman, J. Phys. Chem. 97 (1993) 7711.
[47] A. Bensalem, J.C. Muller, D. Tessier, F. Bozon-Verduraz, J. Chem. Soc. Faraday Trans. 92 (1996) 3233.
[48] J.A. Anderson, C. Márquez-Alvarez, M.J. López-Muñoz, I. Rodríguez-Ramos, A. Guerrero-Ruiz, Appl. Catal. B 14 (1997) 189.
[49] J. Hoffman, I. Meusel, J. Hartmann, J. Libuda, H.-J. Freund, J. Catal. 204 (2001) 378.
[50] A.L. Tarasov, L.K. Przheval'skaya, V.A. Shevts, V.B. Kazanskii, Kinet. Katal. 29 (1989) 1020.
[51] P. Bera, V. Jayaram, G.N. Subbana, M.S. Hegde, J. Catal. 196 (2000) 293.
[52] F. Illas, N. López, A. Clotet, J.M. Ricart, J.C. Conesa, M. Fernández-García, J. Phys. Chem. B 102 (1998) 8017.
[53] K. Wolter, H. Kuhlenbeck, H.-J. Freund, J. Phys. Chem. B 106 (2002) 6723.
[54] R. Di Monte, P. Fornasiero, J. Kašpar, P. Rumori, G. Gubitosa, M. Graziani, Appl. Catal. B 24 (2000) 157.
[55] R. Farrauto, R.M. Heck, Catal. Today 51 (1999) 351.